Available online at www.sciencedirect.com
ScienceDirect
Journal of Power Sources 174 (2007) 554–559
JOURNAL OF POWER SOURCES
www.elsevier.com/locate/jpowsour

Short communication

Material design concept for Fe-substituted Li_2MnO_3-based positive electrodes

Mitsuharu Tabuchi *, Yoko Nabeshima, Kazuaki Ado, Masahiro Shikano, Hiroyuki Kageyama, Kuniaki Tatsumi

National Institute of Advanced Industrial Science and Technology (AIST), 1-8-31 Midorigaoka, Ikeda, Osaka 563-8577, Japan

Available online 3 July 2007

Abstract

Fe-substituted Li_2MnO_3 ($Li_{1+x}(Fe_yMn_{1-y})_{1-x}O_2$, $0 \le x \le 1/3$, $0.3 \le y \le 0.7$) was synthesized using a combination of coprecipitation, hydrothermal, and heat-treatment methods. It exhibits high initial specific capacity greater than 200 mAh g^{-1} and small capacity, which fades up to the 50th cycle (>150 mAh g^{-1} at the 50th cycle) under electrochemical cycle testing at 60 °C. The attractive electrode properties appeared by controlling the chemical composition ($x > 0.05$, $0.3 \le y \le 0.5$) and high specific surface area (>20 m^2 g^{-1}). The Fe-substituted Li_2MnO_3 is an attractive candidate as a novel 3 V-class positive electrode material.

Keywords: Lithium-ion batteries; Fe-substituted; XRD

1. Introduction

Lithium-ion batteries (LIB) are a key energy device, not only for mobile hardware, but also for hybrid electric vehicle (HEV) and load-leveling systems. For such applications, the current positive electrode $LiCoO_2$ is unsuitable because of the uneven distribution of expensive Co sources. Although electrodes based on $LiNiO_2$, $LiNi_{0.5}Mn_{0.5}O_2$, and $LiMn_2O_4$ are candidates, challenges of finding novel iron-oxide-based positive electrode are more attractive because of the relative abundance of Fe sources. We determined Fe-substituted Li_2MnO_3 ($Li_{1+x}(Fe_yMn_{1-y})_{1-x}O_2$, $0 < x < 1/3$, $0 < y < 1$) as a novel positive electrode material [1] because of the appearance of Fe^{3+}/Fe^{4+} redox around 4 V. However, the observed discharge capacity of $Li_{1.2}(Fe_{0.5}Mn_{0.5})_{0.8}O_2$ ($Li_{1.2}Fe_{0.4}Mn_{0.4}O_2$) was less than 100 mAh g^{-1} in spite of the efforts of careful control of chemical composition and preparation conditions [1–3]. That low discharge capacity might originate from the small ideal capacity (127 mAh g^{-1}) of $Li_{1.2}Fe_{0.4}Mn_{0.4}O_2$ and electrochemically-inactive characteristics of $LiFeO_2$. This material has a large specific capacity: it is greater than 200 mAh g^{-1} at 60 °C [4]. This study is intended to discover the factors that are responsible for their electrochemical properties to construct a material design concept for this material.

2. Experiment

Coprecipitation, mixed-alkaline hydrothermal [5] and heat treatment processes named as steps (1)–(3) were necessary for obtaining homogeneous samples.

In step (1), 0.125 mol (50.50 g) of $Fe(NO_3)_3{\cdot}9H_2O$ (>99.9% purity; Wako Pure Chemical Industries) and 0.125 mol (24.74 g) of $MnCl_2{\cdot}4H_2O$ (>99% purity; Wako Pure Chemical Industries) were dissolved into 500 ml of distilled water for preparation of Li_{1+x} $(Fe_{0.5}Mn_{0.5})_{1-x}O_2$. The Fe/(Fe + Mn) ratio (y) in samples was adjusted by changing the amounts of $Fe(NO_3)_3{\cdot}9H_2O$ and $MnCl_2{\cdot}4H_2O$. The LiOH aqueous solution was prepared by dissolving 50 g of $LiOH{\cdot}H_2O$ into 500 ml of distilled water. The LiOH solution was poured into a Ti beaker; then 150 ml of ethanol was added to prevent freezing of the solution during coprecipitation. The Ti beaker was set in a temperature-controlled bath filled with antifreeze liquid and cooled to −10 °C. After cooling, that Fe–Mn mixed solution was added to the LiOH solution with stirring for 2–3 h. The resultant Fe–Mn coprecipitate was aged with stirring under air bubbling overnight at room temperature. The coprecipitate was isolated through a filtration process for the hydrothermal process.

* Corresponding author.
E-mail address: m-tabuchi@aist.go.jp (M. Tabuchi).

0378-7753/$ – see front matter © 2007 Elsevier B.V. All rights reserved.
doi:10.1016/j.jpowsour.2007.06.247

In step (2), 309 g of KOH (Wako Pure Chemical Industries), 50 g of $LiOH{\cdot}H_2O$ and 50 g of $KClO_3$ are mixed with 500 ml of distilled water and the Mn–Fe coprecipitate into a polytetrafluoroethylene beaker for mixed alkaline hydrothermal reaction at 220 °C for 8 h. The products were isolated through repeated washing with distilled water, filtration, and drying overnight. The hydrothermally obtained samples with $y = 0.3$, 0.4, 0.5, 0.6 and 0.7 were named respectively as Y03-H, Y04-H, Y05-H, Y06-H and Y07-H.

In step (3), the hydrothermally obtained sample, Y05-H (0.25 mol) was mixed with 100 ml of LiOH solution including 0.125 mol of $LiOH{\cdot}H_2O$ (5.25 g). After drying at 100 °C overnight and grinding, the mixture was heat-treated in air to target temperatures of 750, 800, 850 or 900 °C for 1 h. After keeping the sample at the target temperature for 1 min, it was cooled immediately to room temperature in a furnace. The final products were named Y05-750, Y05-800, Y05-850 and Y05-900 corresponding to their target temperatures. Unreacted lithium carbonate and hydroxide were eliminated through rinsing with distilled water, filtration, and subsequent drying processes.

Purity and 3d metal distribution analyses of all samples were characterized using X-ray diffraction (XRD) measurements (Rotaflex RU-200B/RINT; Rigaku) using monochromatized Cu Kα radiation within the 2θ of 10–125°. The diffraction angle was calibrated using silicon powder (SRM 640c) as an external standard. The RIETAN-2000 program was used for structural refinement with X-ray Rietveld analysis [6]. Elemental analyses of Li, Fe and Mn were performed using inductively coupled plasma (ICP) spectrometry to estimate their chemical formula. The primary and secondary particle size and shape were observed using scanning electron microscopy (SEM, JSM-6390; JEOL) with LaB_6 filament. The specific surface area (S) was measured using a BET surface area analyzer (Flowsorb 2300; Micrometrics Inc.).

Table 1
The nominal and observed excess amount of Li (x) and Fe content (y) values calculated from elemental analysis and specific surface area (S) data for (a) hydrothermally obtained and (b) heat-treated samples

Sample	Nominal		Observed		S ($m^2\ g^{-1}$)
	x[a]	y	x	y	
(a)					
Y03-H	0.259	0.30	0.128(8)	0.299(4)	39.1
Y04-H	0.231	0.40	0.112(11)	0.398(13)	33.6
Y05-H	0.200	0.50	0.096(10)	0.496(8)	35.3
Y06-H	0.167	0.60	0.039(12)	0.595(16)	41.2
Y07-H	0.130	0.70	0.000(11)	0.702(17)	26.8
(b)					
Y05-H	0.2	0.5	0.096(10)	0.496(8)	35.3
Y05-750	0.2	0.5	0.178(3)	0.502(4)	31.1
Y05-800	0.2	0.5	0.184(8)	0.505(9)	25.8
Y05-850	0.2	0.5	0.202(5)	0.505(10)	21.8
Y05-900	0.2	0.5	0.203(9)	0.505(19)	17.1

[a] The value can be calculated by assuming that only trivalent Fe and tetravalent Mn ions exist in all samples.

Charge and discharge tests were undertaken using a positive electrode comprising the sample (20 mg) acetylene black (5 mg) and polytetrafluoroethylene powder (0.5 mg) under two voltage ranges from 2.0 to 4.5 or 4.8 V against Li metal negative electrode at a fixed current density (42.5 mA g^{-1}). That corresponds to a 1/3C rate for the ideal capacity (127 mAh g^{-1}), which was calculated by assuming that 0.4Li was extracted electrochemically according to the chemical formula $Li_{1.2}Fe_{0.4}Mn_{0.4}O_2$

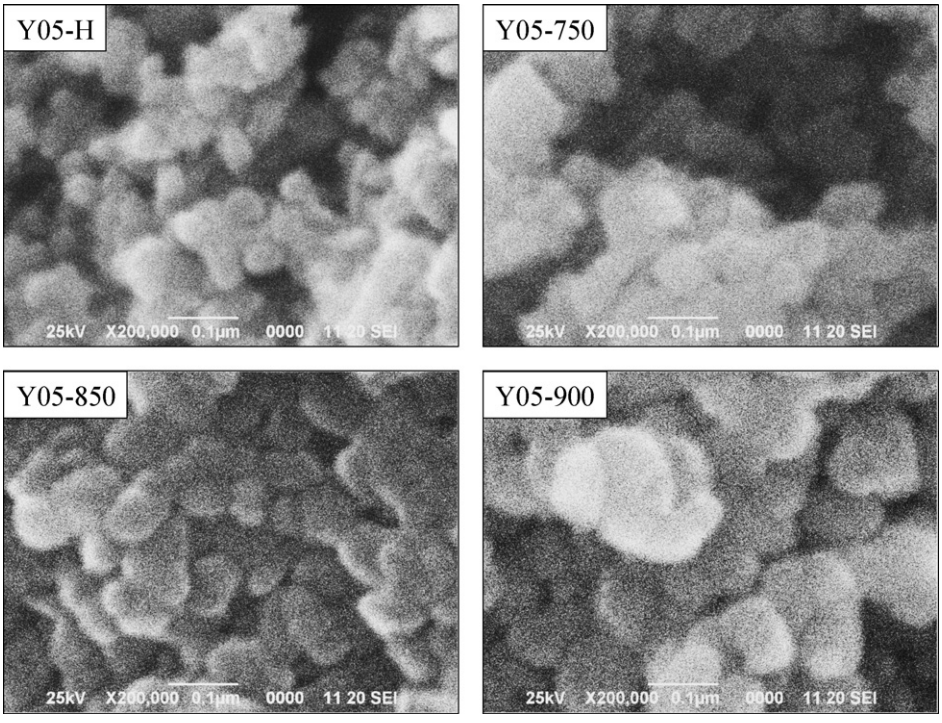

Fig. 1. SEM photographs for hydrothermally obtained (Y05-H) and heat-treated samples with $y = 0.5$ (Y05-750, Y05-850 and Y05-900) under different heat-treatment temperatures: 750, 850 and 900 °C.

Table 2
Structural analysis data for (a) hydrothermally obtained and (b) heat-treated samples

Sample	Layered rock-salt ($R\bar{3}m$) phase ($(Li_{1-h}M_h)_{3a}[M_iLi_{1-i}]_{3b}(M_j)_{6c}O_2$)							Cubic rock-salt ($Fm\bar{3}m$) phase ($(Li_{2-k}M_k)_{4a}O_2$)		
	Mass fraction	a (Å)	c (Å)	h[a]	i[a]	j[a]	$h+i+j$	Mass fraction	a (Å)	k[b]
(a)										
Y03-H	0.8434	2.8711(4)	14.2822(18)	0.041(4)	0.655(8)	0.046(2)	0.742(14)	0.1566	4.0865(13)	0.81(4)
Y04-H	0.6376	2.8825(5)	14.306(2)	0.075(7)	0.728(7)	0.064(3)	0.867(17)	0.3624	4.0973(7)	0.742(18)
Y05-H	0.5946	2.8893(5)	14.330(2)	0.062(7)	0.720(10)	0.059(3)	0.84(2)	0.4054	4.1148(6)	0.804(14)
Y06-H	0.4407	2.8960(10)	14.316(4)	0.074(13)	0.778(19)	0.100(6)	0.95(4)	0.5593	4.1196(4)	0.766(10)
Y07-H	0.2232	2.917(4)	14.312(11)	0 (fixed)	0.65(5)	0.33(3)	0.98(7)	0.7768	4.1309(2)	0.836(5)
(b)										
Y05-H	0.5946	2.8893(5)	14.330(2)	0.062(7)	0.720(10)	0.059(3)	0.84(2)	0.4054	4.1148(6)	0.804(14)
Y05-750	0.6827	2.8884(4)	14.3133(16)	0.032(5)	0.727(11)	0.023(3)	0.782(19)	0.3173	4.1036(8)	0.70(2)
Y05-800	0.7040	2.8887(4)	14.3162(15)	0.053(5)	0.770(10)	0.027(3)	0.850(18)	0.2960	4.1071(8)	0.76(2)
Y05-850	0.7661	2.8854(3)	14.2964(14)	0.055(4)	0.757(8)	0.023(3)	0.835(15)	0.2339	4.1035(7)	0.74(2)
Y05-900	0.7542	2.8854(3)	14.2985(13)	0.062(3)	0.757(7)	0.019(2)	0.838(12)	0.2458	4.1020(6)	0.73(2)

[a] The 3d metal contents according to the chemical formula on 3a (0, 0, 0), 3b (0, 0, 1/2) and 6c (0, 0, z) (z = ca. 3/8) sites expressed respectively as the h, i and j values. The h, i and j values were related to the occupancy (g) of 3d metal ions on three different crystallographic sites as $h = g_{3a}$, $i = g_{3b}$ and $j = 2g_{6c}$. The h value for Y07-H was fixed to zero to give a negative value during the refinement process.

[b] The Fe and Mn contents according to the chemical formula on 4a (0, 0, 0) site are expressed respectively as the k values. The k values were related to the occupancy (g) of Fe and Mn ions on 4a sites as $k = 2g_{4a}$.

because of the oxidation of all Fe^{3+} to Fe^{4+}. The $LiPF_6$ was dissolved in EC and DEC mixed solvent (Tomiyama Pure Chemical Industries) for use as an electrolyte. Cell testing started from charging.

3. Results and discussion

The effect of chemical composition (Fe content) was first examined using a series of hydrothermally obtained samples, from Y03-H to Y07-H. Elemental analyses revealed that their chemical formulae were close to the expected composition, $Li_{1+x}(Fe_yMn_{1-y})_{1-x}O_2$, $0 < x < 1/3$, $0 < y < 1$ (Table 1(a)). The small observed x values, compared to nominal ones, are inferred to originate from the leaving Li ion during washing.

All samples showed particle agglomeration (1–100 μm) of small primary particles (<0.1 μm) (Fig. 1). The primary particle size was nearly constant, except for Y07-H, as implied by their specific surface area data (Table 1(a)).

Although all XRD peaks for Y05-H were indexed using a layered rock-salt unit cell ($R\bar{3}m$), some peaks tailed to a higher 2θ angle (Fig. 2(a)). X-ray Rietveld analysis revealed that the sample consisted of 59 wt.% layered ($R\bar{3}m$) and 41 wt.% cubic ($Fm\bar{3}m$) rock-salt phases (Table 2(a)). The cubic rock-salt phase content was increased with increasing Fe content, y, indicating that α-$LiFeO_2$-based solid solution coexists with a Li_2MnO_3-based one. The observed 3d metal contents per chemical formula for both phases ($h+i+j$ and k values in Table 2(a) were interme-

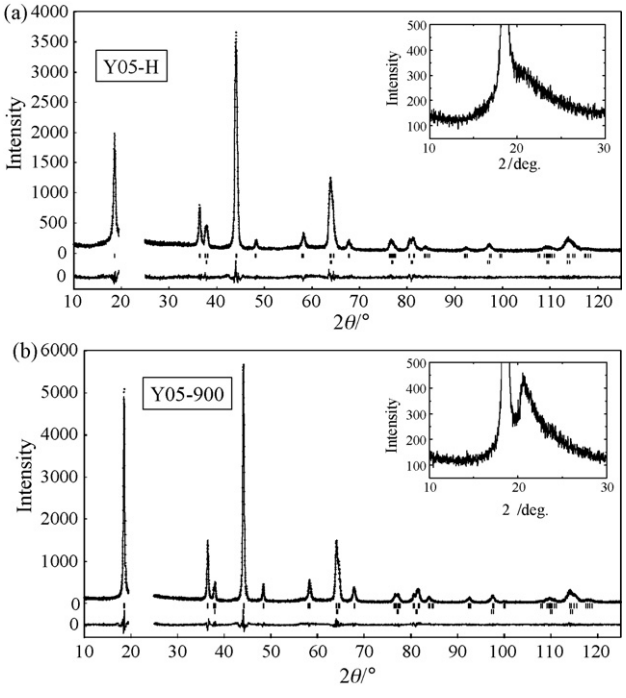

Fig. 2. Observed (+) and calculated (solid curve) X-ray diffraction patterns for a hydrothermally obtained sample with $y = 0.5$, (Y05-H) (a) and for a heat-treated one at 900 °C (Y05-900) (b). X-ray diffraction patterns ($2\theta = 10$–$30°$) were inserted into the figure.

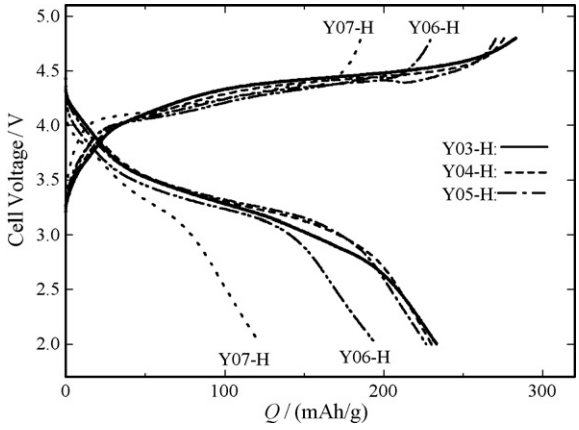

Fig. 3. Initial charge and discharge curves at 60 °C for hydrothermally obtained samples with different Fe contents. The symbol Q was used to represent specific capacity data.

diate between the expected values (0.67 and 1.00) for two end members (Li_2MnO_3 and $LiFeO_2$). The $h+i+j$ and k values were defined based on the sum of occupancy of three crystallographic sites, 3a, 3b and 6c for layered rock-salt phase, and were based, respectively on occupancy of 4a for cubic rock-salt phases. The result indicates the formation of Fe^{3+}-substituted Li_2MnO_3 ($R\bar{3}m$) and Mn^{4+}-substituted $LiFeO_2$ ($Fm\bar{3}m$). The two-phase trend was consistent with the proposed model for Cr-substituted Li_2MnO_3 by solid-state ^{6}Li NMR study [7]. Although, we say no additional comments concerning about homogeneity of sample, we will show the result about the sample quality by other analysis technique in the forthcoming paper. In the structural model of layered rock-salt phase, a small amount of 3d metal might exist on a distorted tetrahedral (6c, (0, 0, z), z = ca. 3/8) site adjacent Li ion in the 3a site. The amount of 3d metal on the 6c site according to the chemical formula (j value in Table 2(a)) increased with Fe content, suggesting that Fe ions occupy the tetrahedral 6c site. The j value decreased after heat-treatment (Table 2(b)), indicating that the unusual 3d metal distribution of layered rock-salt phase might be stabilized by the hydrothermal reaction.

The charge–discharge curves for hydrothermally obtained samples (Fig. 3) showed that they are considered as a 3 V-class positive electrode with high charge and discharge capacities. The maximum discharge capacity (233 mAh g^{-1}) was shown for Y03-H (Table 3(a)). Although, a high discharge capacity (>225 mAh g^{-1}) was attained at $y \leq 0.5$, the capacity decreased drastically for $y = 0.6$ and greater. The observed initial specific capacities depend on excess amounts of Li, x (Fig. 4) and fraction of layered rock-salt phase (Fig. 5). The careful control of sample composition and structure such as low Fe ($0.3 \leq y \leq 0.5$) and high Li contents ($x > 0.05$) and high fraction of layered rock-salt phase (>55%) are necessary for high initial specific capacities greater than 200 mAh g^{-1}. The discharge capacity fading behavior (Fig. 6) indicated that capacity fading is considerable for samples withy less than 0.6. Heat-treated samples with $y = 0.5$ (Y05-750 to Y05-900) were therefore prepared.

All heat-treated samples showed higher x (>0.17) values and fractions of layered rock-salt phase (>68 wt.%) than those for the hydrothermally obtained one (Table 2(b)) because of the crystal growth of each primary particle (Figs. 1 and 2) and the compensation of loss of Li during washing by reaction with LiOH. In fact, XRD peaks for Y05-900 (Fig. 2 (b)) become sharp compared with those for Y05-H.

Initial charge and discharge curves for these samples are shown in Fig. 7 for voltages of 2.0–4.5 V. The upper voltage can be reduced from 4.8 to 4.5 V through reduction of the charging voltage with increasing Fe contents (Fig. 3).

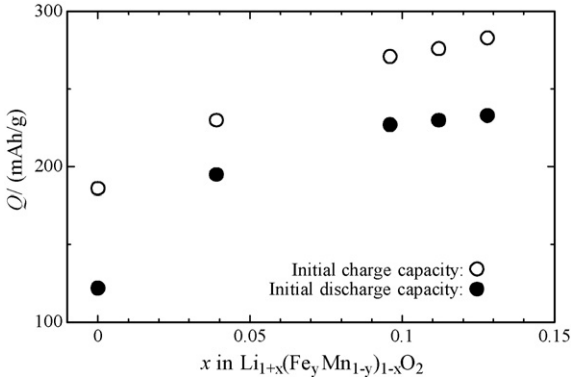

Fig. 4. Plots of initial charge (◯) and discharge (●) capacities (Q) against the excess amount of Li (x) per chemical formula ($Li_{1+x}(Fe_yMn_{1-y})_{1-x}O_2$) for hydrothermally obtained samples.

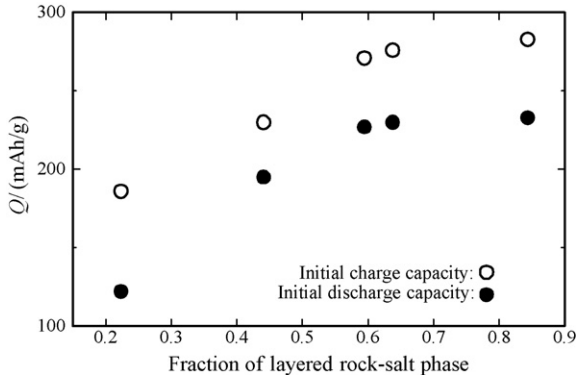

Fig. 5. Plots of initial charge (◯) and discharge (●) capacities (Q) against the fraction of layered rock-salt phase for hydrothermally obtained samples.

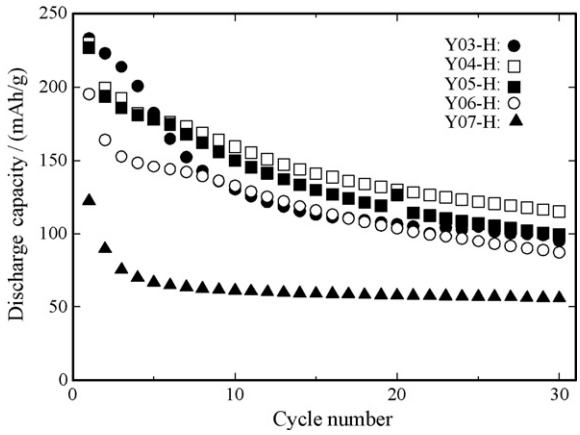

Fig. 6. Discharge capacity fading behavior for hydrothermally obtained samples with different Fe contents, y.

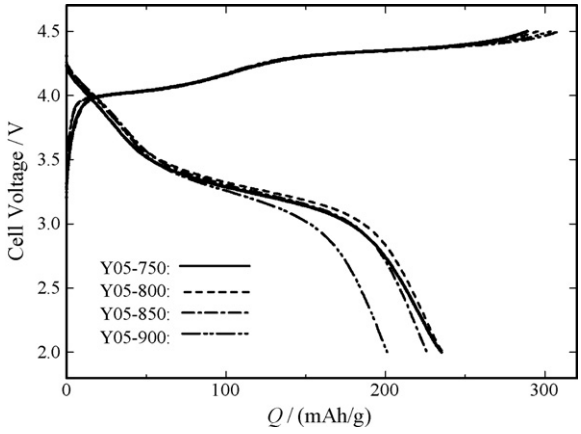

Fig. 7. Initial charge and discharge curves at 60 °C for heat-treated samples with $y = 0.5$ obtained under different firing temperatures. The symbol Q was used to show specific capacity data.

Table 3
Initial and 10th charge (Q_{1c} and Q_{10c}) and discharge (Q_{1d} and Q_{10d}) data (a) between 2.0 and 4.8 V for hydrothermally obtained samples and (b) between 2.0 and 4.5 V for heat-treated samples

Sample	Initial charge and discharge data					10th discharge data	
	Q_{1c} (mAh g^{-1})	Q_{1d} (mAh g^{-1})	$(100Q_{1d}/Q_{1c})$ (%)	$V_{average}$ (V)	$V_{average}Q_{1d}$ (mW h g^{-1})	Q_{10d} (mAh g^{-1})	$(100Q_{10d}/Q_{1d})$ (%)
(a)							
Y03-H	283	233	82.4	3.17	740	130	55.7
Y04-H	276	230	83.4	3.23	742	159	69.2
Y05-H	271	227	83.8	3.23	732	150	66.1
Y06-H	230	195	84.8	3.17	618	133	67.9
Y07-H	186	122	65.7	3.13	383	61	50.1
(b)							
Y05-750	289	235	81.4	3.21	756	185	78.7
Y05-800	296	236	79.8	3.26	769	186	78.9
Y05-850	309	226	73.2	3.27	739	175	77.5
Y05-900	304	201	66.2	3.26	655	156	77.4

Unexpectedly, the initial discharge capacity and efficiency decreased drastically with firing temperatures greater than 850 °C. We plot these electrochemical data against the specific surface area to explain this phenomenon (Fig. 8). The two plots show that high specific surface area (>20 m^2 g^{-1}) can contribute to improvement of electrochemical properties (Tables 1(b) and 3(b)). Discharge capacity fading behavior (Fig. 9) is sensitive to the heating temperature. Sample Y05-850 exhibited a best-cycle performance. The discharge capacity of this sample was greater than 150 mAh g^{-1} at the 50th cycle. Although Y05-900 shows similar capacity-fading behavior to that of Y05-850, the discharge capacity was small because of grain growth.

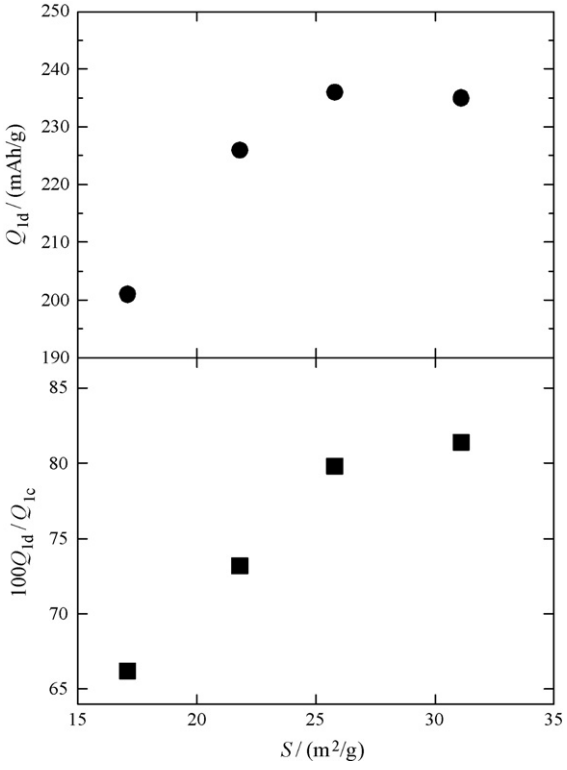

Fig. 8. Plots of initial discharge (●) and efficiency (■) against the specific surface area (S) for heat-treated samples.

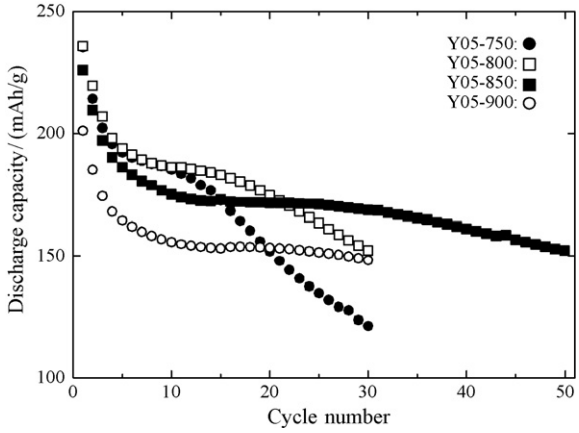

Fig. 9. Discharge capacity fading behavior for heat-treated samples with $y = 0.5$ obtained under different firing temperatures.

4. Conclusion

These results show that Fe-substituted Li_2MnO_3 is as attractive a material for 3 V-class positive electrodes as $LiFePO_4$, as indicated by its high specific capacity above 200 mAh g^{-1}, if the iron content, Fe/(Fe + Mn) is adjusted between 0.3 and 0.5. Although the high initial charge capacity was governed mainly by two factors, high Li content ($x > 0.05$) and high fraction of layered rock-salt phase (>55%), the high initial discharge capacity and efficiency were supported by their high specific surface area (>20 m^2 g^{-1}, or small primary particle size) in addition to the above two factors.

From these summary, we noticed that the electrochemical reactions of this positive electrode material must be caused on the vicinity of the surface, or shallow reaction depth (<50 nm) and that Fe ions can act as an effective activator to bring Li ions in Li_2MnO_3 into electrochemical reactions. Although further analysis to know the charge and discharge mechanism must be needed, Fe^{3+} ion is an important doping element as well as Cr^{3+}, Co^{3+}, and Ni^{2+} ions into Li_2MnO_3 structure if suitable preparation conditions were selected.

Acknowledgements

This work is supported financially by NEDO and METI in "Development of lithium battery technology for use in fuel cell vehicles, FY2002-FY2006". One author (M.T.) expresses his gratitude to Dr. Tatsuya Nakamura (University of Hyogo) for fruitful discussions.

References

[1] M. Tabuchi, A. Nakashima, H. Shigemura, K. Ado, H. Kobayashi, H. Sakaebe, H. Kageyama, T. Nakamura, M. Kohzaki, A. Hirano, R. Kanno, J. Electrochem. Soc. 149 (5) (2002) A509–A524.

[2] M. Tabuchi, A. Nakashima, K. Ado, H. Sakaebe, H. Kobayashi, H. Kageyama, K. Tatsumi, Y. Kobayashi, S. Seki, A. Yamanaka, J. Power Sources 146 (2005) 287–293.

[3] M. Tabuchi, A. Nakashima, K. Ado, H. Kageyama, K. Tatsumi, Chem. Mater. 17 (2005) 4668–4677.

[4] M. Tabuchi, M. Shikano, Y. Nabeshima, K. Ado, H. Kageyama, H. Sakaebe, K. Tatsumi, Extended Abstract for the 46th Battery Symposium in Japan, Nagoya 3B01, 2005, pp. 234–235 (in Japanese).

[5] K. Ado, M. Tabuchi, H. Kobayashi, H. Kageyama, O. Nakamura, Y. Inaba, R. Kanno, M. Takagi, Y. Takeda, J. Electrochem. Soc. 144 (7) (1997) L177–L180.

[6] F. Izumi, T. Ikeda, Mater. Sci. Forum 198 (2000) 321–324.

[7] C. Pan, Y.J. Lee, B. Ammundsen, C.P. Grey, Chem. Mater. 14 (2002) 2289–2299.